scientific reports

Check for updates

OPEN

Real-time imaging on a microwell device allows first insights into the embryonic development of the ubiquitous and notorious scabies parasite

Gangi R. Samarawickrama[1,2], Deepani D. Fernando[1,2], Tam Hong Nguyen[3], Satomi Okano[4], Gunter Hartel[4], Malcolm K. Jones[1,2] & Katja Fischer[1,2]✉

Scabies is a common and highly contagious skin disease, caused by obligate parasitic burrowing mites (*Sarcoptes scabiei*). Current drugs have a short skin half-life and are ineffective against the egg stages of the parasite. Novel scabicides are needed that target eggs as well as motile mites, therefore understanding the egg structure and embryogenesis is crucial in developing ovicidal drugs. However, the embryogenesis of mites and specifically of *S. scabiei* is not well understood. To address this, we utilized a unique porcine scabies model, representing a nearly unlimited source of parasites that allowed us perform a descriptive embryonic development study. We designed and custom-fabricated a medium-throughput microwell device to confine individual *S. scabiei* eggs for automated microscopic observation over time. Using time-lapse microscopy, we recorded the development of 40 individual eggs, generating the first comprehensive timeline of *S. scabiei* embryogenesis and revealing distinct morphological stages and developmental dynamics.

Keywords Sarcoptes scabiei, Parasitic mite, Egg and embryogenesis, Scabies

Scabies is one of the most common dermatological conditions globally and is particularly prevalent in economically disadvantaged tropical settings. With at least 200 million people being affected at any one time, scabies disease and its complications represent a significant public health burden worldwide[1]. Excretions of the burrowing mites trigger intense pruritus, the hallmark symptom of scabies. Scratching disturbs the epithelial skin barrier and provides an opportunity for secondary bacterial infections to establish. Two main pathogens associated with scabies are Group A *Streptococcus* (GAS) and *Staphylococcus aureus*[2] which can cause localized pyoderma and cellulitis or serious systemic illness, including bacteraemia, septicaemia, heart or kidney diseases[3,4].

Scabies mites are obligate epidermal parasites that undergo four main developmental stages - egg, larva, nymph, and adult - in a direct life cycle typical of astigmatid mites[5,6]. The largest stage, the adult female mite, measures 0.3 to 0.5 mm in length and the egg, as the smallest stage, just under 0.2 mm. Mated females burrow into the skin to lay two to three eggs daily, producing 60–100 eggs over their 1-1.5-month lifespan, thereby rapidly increasing parasite load. Eggs hatch within 3 days, and six-legged larvae progress through eight-legged protonymph and tritonymph stages before reaching adulthood in approximately 10–17 days. Reported life-cycle durations vary across host species and studies (7–21 days in humans; 10–15 days in animals), likely reflecting variations in environmental conditions and host species physiology.

Although the burden of scabies on humans and animals is well recognized and basic mite biology has been established[1,6], much of the molecular pathobiology remains to be elucidated. Due to this lack of knowledge, molecular diagnostic tools are still in development[7], there is no vaccine to prevent scabies[8], and relatively few therapeutic regimes are available to treat scabies[1].

[1]Infection and Inflammation Program, QIMR Berghofer, Herston, Brisbane, Australia. [2]School of Veterinary Science, University of Queensland, Gatton Campus, Gatton, Brisbane, Australia. [3]Microscopy and Spatial Cell Biology Facility, QIMR Berghofer, Herston, Brisbane, Australia. [4]Statistics Unit, QIMR Berghofer, Herston, Brisbane, Australia. ✉email: katja.fischer@qimrb.edu.au

Research has been hampered by poor access to the parasites. Most patients present with common scabies where the mite load is typically under 15 parasites per host[1]. Occasionally, large numbers of mites can be obtained from a patient with crusted scabies, but for ethical reasons and practicability, extensive research studies can't be performed easily[9]. Furthermore, the parasite is difficult to study ex vivo, as it cannot survive outside the host skin for more than a few days, depending on temperature and humidity[10], and it cannot be cultivated in vitro[6].

Almost all drugs in use kill the motile stages of the parasite by affecting their nerve and muscle functions[11,12], but appear to be ineffective on *S. scabiei* eggs[13]. The absence of ovicidal activity is a problem because many drugs used as scabicides have a short half-life in the skin. For example, the skin half-life of ivermectin is about 24 h[14] but the time from oviposition to hatching of a *S. scabiei* egg is estimated to be longer than 50 h[6]. Consequently, embryos unaffected by the treatment will hatch into a new generation of larvae. These larvae survive because at the time they hatch the drug concentration in skin has become too low to be effective, and hence the infestation continues. Repeat treatments are mandatory to terminate the infection, however non-compliance to repeat treatments is a major problem in scabies management at individual, household and community levels, and often leads to treatment failures[15,16].

In addition to the eggs being unaffected by non-ovicidal drugs, they are also the "amplification stage" in the scabies life cycle. Hence, it is highly important to understand the biology of the scabies egg stage in order to find new drugs with ovicidal properties. While there is some literature on the structure of the *S. scabiei* egg and egg shell[17–19], a small number of reports that are available, illustrate only a few single embryonic stages that were captured using bright field[20–22], fluorescence[23] or electron[17] microscopic techniques. However, none of these studies provided a comprehensive overview of scabies mite embryogenesis in real-time.

Varieties of *S. scabiei* from many mammalian hosts have been found to be morphologically identical[24–26] and, while not known to date, they likely share a highly similar if not identical embryology. Hence, we sourced the mites and eggs utilised in this study from an established porcine model[24]. We developed a microwell platform enabling medium-throughput, automated microscopy of *S. scabiei* eggs for robust, statistically valid data collection. Using time-lapse imaging, we captured the dynamic sequence of *S. scabiei* embryogenesis and provide a detailed temporal reference atlas observable in real time.

Results

A microwell platform for time-lapse imaging of developing acarid eggs

A custom-designed and manually fabricated microgrid mounted on a microscopic slide was developed to enable microscopic time-lapse imaging of *S. scabiei* eggs within a single experiment (Fig. 1a and b). The device is compatible with the automated X-Y stage of an inverted microscope imaging system equipped with an environmental incubator that maintains conditions of 37 °C, 5% CO_2, 20% O_2 and 80% humidity. A Z-stack flat focus feature was used to acquire images in the z-axis at seven focal points in a range of 53–55 µm. The microgrid comprises two layers: an upper thick layer containing six independent primary wells, each subdivided into 20 smaller secondary wells within a thinner lower layer. This configuration accommodates up to 120 *S. scabiei* eggs per experiment, with one egg per secondary well. When mounted on an automated stage, individual eggs can be sequentially imaged at defined intervals throughout embryonic development. This setup enables longitudinal microscopic observation of a statistically robust number of individual eggs under multiple experimental conditions within a single run.

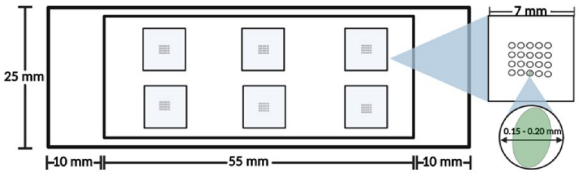

(a)

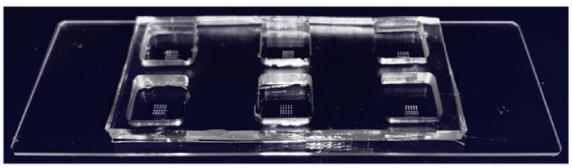

(b)

Fig. 1. Design (**a**) and prototype (**b**) of the microwell device developed for time-lapse microscopy. The device consists of six square primary wells (7 × 7 × 2 mm), each accommodating 20 circular secondary wells (150–200 µm diameter, 200 µm depth) arranged in four rows of five wells each and centered within each primary well. The stacked primary and secondary wells were bonded to each other and to an underlying quartz microscope slide (75 × 25 × 0.5 mm). A schematic green ellipse illustrates egg size relative to the size of the secondary well.

Time-lapse documentation of *S. scabiei* embryogenesis

The transparent chorion of the scabies egg allows visualization of embryonic development without prior preparation. Time-lapse photography was used to generate time-lapse sequences of live embryos under the microscope. A link to these videos is provided at https://doi.org/10.48610/fe96dbe to be watched using FIJI Image][27]. Time-lapse videos of 40 eggs were generated in two experiments representing two biological replicates. None of the eggs moved out of focus within the confined secondary wells during the experiments. Hence, it was possible to retrospectively determine the anterior and posterior ends of the eggs, as well as the dorsal and ventral planes of most, based on the direction of limb development and limb movements. An overview of the positions of the observed eggs is provided in Supplementary Table S1.

In two independent experiments performed on separate days a total of 40 eggs (2 × 20) were monitored using the microwell platform and time-lapse microscopy. Gravid female mites were allowed to oviposit for 30 min at room temperature (RT). Loading 20 freshly laid eggs and configuring the microscope required approximately 1.5 h, resulting in an estimated 2-hour interval between oviposition and the start of imaging. Out of 40 eggs, two could not be analysed due to technical issues, and two additional eggs degenerated early during the gastrula stage. The remaining 36 eggs developed into vital, motile larvae. Ten of these larvae did not fully emerge from the egg shell, but displayed motility comparable to those that hatched completely. Four eggs, loaded last during the setup, produced healthy larvae that hatched shortly after the scheduled observation period, corresponding to four lines terminating at events 36–39 in Fig. 2.

A staging system for *S. scabiei* embryogenesis

Under the set in vitro conditions in the microwell device, the median observation time for scabies embryogenesis was slightly less than 58 h, which after adding the approximate two hours spent for loading, amounted to a time after egg laying (AEL) of just under 60 h. In total, 42 morphological alterations and embryonic movements (E1-E42) were observed during six distinct phases (Fig. 3). To visualize the duration and variation of stages, we graphed the events observed individually for each egg, plotting every observed change throughout embryogenesis against the start time (Fig. 2). A steep rise of the curve from events E1 to E16 reflects a rapid succession of changes during the first 10 h of embryo development (Fig. 2). During the differentiation of the embryo and the development of mite features in later phases, the curve gradually plateaued, i.e. observable morphological events were spread over longer periods of time. From event E34 (first embryo movements) onwards, a distinct increase in the variation of duration of dynamic events between individual eggs was observed.

The imaging data were used to produce a first temporal reference staging system of morphological development during *S. scabiei* embryogenesis (Table S2). Selected characteristic morphological features observed during embryogenesis are shown in Fig. 3.

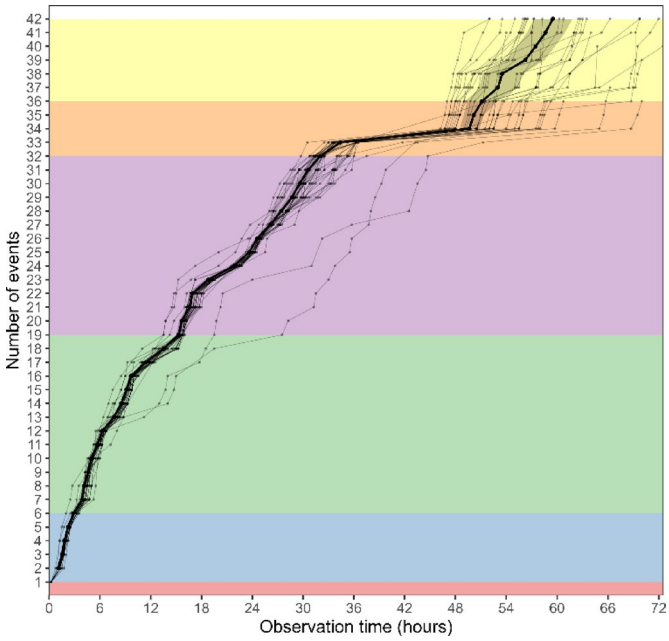

Fig. 2. Temporal progression of scabies mite embryogenesis. Morphological events and egg movements observed during embryogenesis were plotted against time of occurrence. The medium observation time with IQR (interquartile range) from 36 eggs is indicated in grey. An estimated (censoring-adjusted) median and 95% CI from 22 eggs that were observed to exit the egg shell completely is indicated in black. Background colours denote the main embryonic stages: early cell divisions (red), blastula (blue), gastrula (green), initial differentiation (violet), further development (orange), and hatching (yellow).

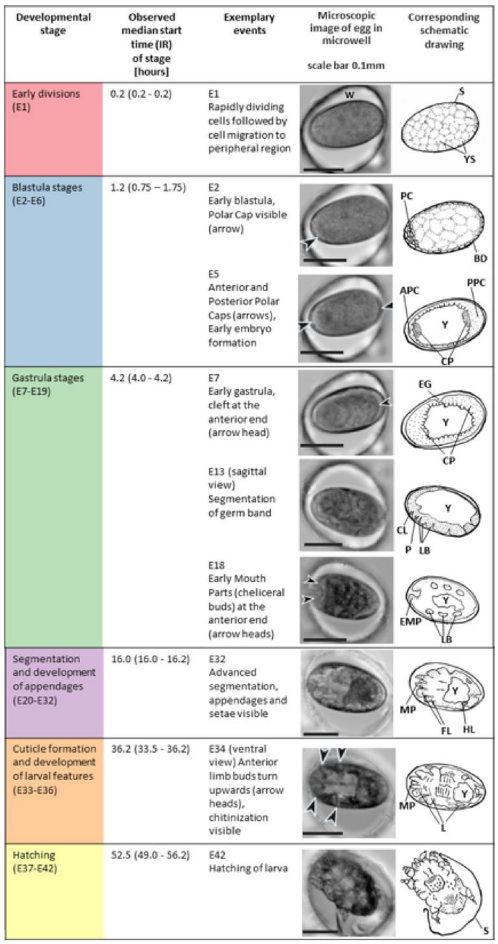

Fig. 3. Embryogenesis of *S. scabiei*. Selected developmental stages are presented and a corresponding schematic illustration is included. The median observation time from start of imaging to start of stage is indicated. IR, Interquartile Range; W, Microwell; S, Shell; YS, Yolk Spherules; BD, Blastoderm; PC, Polar Cap; APC, Anterior Polar Cap; PPC, Posterior Polar Cap; CP, Cell Proliferation; Y, Yolk; EG, Early Gastrularisation; CL, Cephalic Lobe, P, Pedipalp; EMP, Early Mouth Parts; LB, Limb Buds; HL, Hind Limbs; FL, Front Limbs, L, Limbs. Imaging was performed using phase contrast microscopy. The objective used was a 20X PlanFL (fluorite) NA0.4. 20x magnification was used to ensure that the whole scabies egg could fit into one field of view to track morphological changes over time. Z-stack images were acquired as part of the experiment protocol and best focus planes were selected to present. The scale bar corresponds to 0.1 mm. More details are provided in Supplemental files and time lapse movie files at https://doi.org/10.48610/fe96dbe .

Early divisions Freshly laid eggs have an elongated ellipsoid shape evenly filled with numerous yolk droplets contained by the egg shell. After placing the eggs in the microwell device and starting the time-lapse microscopy, our first observations were the peripheral cytoplasm forming around the central yolk within the eggs (E1, Fig. 3). While the initial mitotic divisions could not be observed in our system, an advanced stage of the superficial division process (E1) could be captured in most eggs.

Blastula stages The blastula (E2 - E6) commenced with the appearance of the blastoderm and the emergence of posterior polar cap (E2, Fig. 3), followed by the appearance of a transverse furrow, a grove or indentation forming across the embryo's surface (E3, Table S2), dividing the embryo into posterior and anterior portions. Polar caps (E4) and subsequently anterior posterior proliferation (E5) were observed. Cells migrating to the posterior pole (E6) indicated the finishing point of blastula stage.

Gastrula stages Further cellularization of the blastoderm was observed, initiating the gastrula formation in a series of cumulative events (E7–19, Table S2). Early gastrula (E7) commenced with an opening at the mid to anterior part of the embryo. We next observed continued cellularization (E8) and transverse indentations across the anterior and posterior halves of the embryo (E9). Two openings were seen at the anterior and posterior poles of the embryo (E10). Germ band elongation (E11) was followed by embryo segmentation (E12, E13). Subsequently, germ band retraction initiated (E14) and the embryo rotated relative to the anterior-posterior axis (E15). The stomodeal plate (E16) developed anteriorly, and subsequently a protrusion of the embryo occurred at the posterior pole (E17). Cheliceral buds, the first pair of appendage primordia to form during chelicerate em-

bryogenesis, appeared around the stomodeal plate of the embryo and continued to elongate (E18). The complete gastrula (E19) was observed at the end of this complex cascade of events.

Segmentation and development of appendages The differentiation of larval features began with the appearance of mouth palpi, the second pair of appendage buds located posterior to the cheliceral buds, and advanced body segmentation of the embryo (E20). This was followed by the appearance of the stomodeum (E21), a depression in the oral region of the embryo, followed by stomodeal invagination (E22). Primordial anterior appendages of the embryo were seen, first the pro-head (E23) and then the anterior pairs of limb buds (E24). Mid bilateral furrows were seen at the horizontal axis (E25) followed by more pronounced compartmentalization of the embryo (E26). Advanced anterior limb buds and early mouthparts were observed (E27, E28) and posterior limb buds appeared (E29). Further differentiation simultaneously involved primary appendages; head and elongation of anterior and posterior limb buds in (E30). While the legs were still in a compact anterior arrangement at this stage they started to extend ventrally (E31), ensuring maximum use of limited space inside the egg shell. Setae (hair-like structures) were observed on the limb buds of the embryo for the first time (E32).

Cuticle formation and development of larval features This phase began with the first observation of yolk material appearing within the developing digestive system (E33). Initial embryonic movements were observed in all eggs, marked by upward motion of the anterior limb pair (E34). It remains unclear whether these movements were passive, resulting from growth, or active limb repositioning from a compact anterior clustering of appendages to a differentiated arrangement with the first two limb pairs anterior and the third pair posterior. Patterns of parallel cuticular ridges oriented perpendicular to the longitudinal axis were seen in the cuticle (E35, Fig. 3), an indication of chitinization. The second pair of limbs moved upwards (E35), and soon after synchronized "waving-like" head and limb movements parallel to the egg shell wall were observed (E36).

Hatching In this final phase of embryogenesis (E37-E42), the mass of yolk droplets was no longer visible, suggesting that at this stage the yolk was completely absorbed by vitellophages (E37). Distinct forward-backward rocking movements of embryos were observed (E38), followed by synchronized head and limb waving motions parallel to the eggshell (E39). In four eggs, non-directional movements of embryos (E40) occurred instead of events E36, E38 and E39. Finally, a narrow opening appeared on the anterior eggshell wall (E41), marking the initial rupture that preceded larval emergence and hatching (E42).

Discussion

Comparison with previous embryological studies

Time-lapse analysis of *Sarcoptes scabiei* eggs revealed six main embryonic phases encompassing 42 distinct events. As no detailed descriptions of *S. scabiei* embryogenesis exist, we compared our findings with studies of other arthropods, particularly chelicerates, including mites, ticks, and spiders.

Among arthropods, *Drosophila melanogaster* remains the most comprehensively characterized model for embryogenesis[28,29]. However, the large evolutionary distance between insects and mites limits the relevance of direct comparison. More closely related model species include the spiders *Parasteatoda tepidariorum* and *Cupiennius salei*[30,31], the ticks, *Ixodes scapularis*[32] and *Rhipicephalus microplus*[33], and the mite *Tetranychus urticae*[34]. The latter represents a particularly relevant comparator for *S. scabiei*, as it completes embryonic development within three days.

The advanced cleavage patterns observed (E1) were consistent with those described for other chelicerates, including *T. urticae*[34], *C. salei*[35] and eriophyid mites[36]. Early mitotic cleavage events were not captured in our recordings. Although this may reflect a timing limitation in our experimental setup, even eggs loaded last into the microwells, which would be expected to show at least some initial cleavages, lacked early divisions. This observation suggests that the first mitotic divisions may occur prior to oviposition, as proposed for *Acarus siro*[37], another sarcoptiform mite. Due to the limited visibility of nuclei and membranes in live imaging, synchrony of division could not be assessed. We therefore infer that early divisions likely follow the total cleavage pattern typical of most acari[32,36–38], though this remains to be confirmed.

The onset of the blastula stage, marked by the appearance of anterior and posterior pole caps (E2, E4) resembled descriptions for early embryogenesis of eryophyoid mites[39]. Similarly the cellularized mass at E8 has also paralleled that observed in spider embryos[40], and the segmentation pattern at E12 and E13 was comparable to that described in spiders[41], ticks[32] and other mites[34,42,43]. Subsequent gastrulation events, including germ band retraction (E14), embryo rotation along the longitudinal axis (E15), stomodeal plate formation (E16), posterior ventral protrusion (E17) and appearance of cheliceral claw buds (E18) also mirrored developmental stages in eryophyoid[39] and gamasid[43] mites.

Later morphological features, including cheliceral buds and the body segmentation (E20) were similar to those in harvestmen spider embryos[44]. The stomodeum (E21) corresponded to those described in *C. salei*[35]. The sequential appearance and elongation of anterior and posterior limb buds (E24-E31) were consistent with patterns in gamasid mites[43]. The appearance of the pro-head (E23), bilateral furrows along the left-right axis (E25), clear body segmentation (E26), and developed pro-head and anterior limb buds (E28) resembled observations in tick embryogenesis[33]. The emergence of setae (E32) and subsequent cuticle chitinization paralleled features described in insect[33] and tick[45] embryos.

Technical advances and limitations

Previous studies of arthropod embryogenesis have employed various imaging approaches, including time-lapse[35,46], bright field[47], electron[48] and fluorescence[35,39,46] microscopy. Staining techniques such as fluorescence,

haematoxylin-eosin and immunohistochemistry have further refined cellular and tissue-level resolution[49–51]. Time-lapse microscopy remains particularly valuable for documenting dynamic changes in morphogenesis[35,46,52]. Light microscopy combined with staining methods has enabled characterization of cellular cleavage, tissue differentiation, organogenesis, and protein expression in tick and spider embryos[33,41,53]. In this study we used time-lapse microscopy to capture and quantify the major morphological transitions in *S. scabiei* embryogenesis. While many aspects remain to be described, our data provide the first systematic framework for *S. scabiei* embryonic development.

A standard 96-well plate proved unsuitable for time-lapse microscopy of *S. scabiei* eggs due to focal instability caused by movement of the tiny objects within the large volume. To overcome this, we designed a customized polydimethylsiloxane (PDMS) microwell device that securely confined individual eggs. PDMS was selected for its optical clarity, chemical inertness, and biocompatibility, allowing reliable imaging of up to 120 eggs per experiment.While the confined wells secured the eggs and allowed precision imaging, we hypothesize that incomplete emergence of hatchlings from 10 eggs resulted from spatial restriction within the wells. Also, developmental asynchrony emerged at later stages (E34, ~ 50 h). Asynchronous hatching has also been reported in spider mites (*Tetranychus urticae*, *T. kanzawai*)[54]. In *Neoseiulus womersleyi*, mechanical stimulation was shown to delay hatching[55]. Thus, in our setup, physical contact with well walls or vibration from imaging movements may have produced similar inhibitory cues.

Reported life-cycle lengths for scabies mites vary widely in the literature, reflecting the difficulty of observing mites within host skin and the influence of temperature, humidity, and host species. In vivo, *S. scabiei* var. *canis* completes its life cycle in 10–13 days, with larvae hatching 50–53 h post-oviposition and each stage lasting 2–4 days[56]. Similar durations of the life cycle (10–15 days) have been reported for *S. scabiei* var. *suis* in pigs[57]. No systematic in vitro studies have previously examined *S. scabiei* embryogenesis, but developmental delays relative to in vivo conditions are expected due to differences between in vivo and in vitro conditions, as well as methodological factors such as media composition, light exposure, temperature, and humidity. Accordingly, we imaged two batches of 20 eggs to minimize preparation time and allowed for a long observation period. Nevertheless, the two-hour preparation time prevented us from capturing the earliest two hours of development following oviposition, and a few eggs hatched after the observation period ended. Under our conditions, the average embryonic length (AEL) was approximately 60 h - longer than in vivo estimates[56].

The mortality rate of 5.3% was comparable to previous reports for freshly laid eggs maintained in the dark under similar conditions[57,58]. No medium loss occurred, and temperature remained stable throughout imaging.

This methodological innovation represents a critical step toward advancing scabicide discovery and developmental biology of acarine parasites. However, the discussed limitations underscore the importance of including appropriate internal controls in future experimental applications.

Conclusions and future directions

We established the first live-imaging platform for *S. scabiei* embryogenesis, overcoming key technical obstacles associated with this minute parasitic mite. This work defines a morphological stage system and provides a foundation for future developmental, molecular, and pharmacological investigations.

The microwell system enables medium-throughput imaging of large egg cohorts, facilitating integration with molecular tools such as RNA interference (RNAi), developmental proteo-transcriptomics, and single-cell sequencing. These approaches could elucidate cell lineage trajectories and identify ovicidal drug targets.

Furthermore, this is the first system permitting medium-throughput screening of *S. scabiei* eggs. When combined with time-lapse imaging, it allows direct detection and visualization of drug effects across defined embryonic stages.

With further adaptation, the microwell platform could support broader applications, including drug testing on *S. scabiei* mites themselves and other medically, veterinary, or agriculturally important mite species.

Materials and methods

Fabrication of the microwell device

The microwell was developed in collaboration with Australian National Fabrication Facility (ANFF-Q), University of Queensland, Australia. A combined soft lithography and laser engraving method was used to fabricate the microwell in a silicon-based polymer[58]. The microwell design included two polydimethylsiloxane (PDMS) layers; the upper thick layer with primary wells and the laser engraved bottom thin layer with secondary wells (Fig. 1).

PDMS preparation: PDMS was prepared using silica and agent of silicone (SYLGARD™ 184 silicone elastomer kit, Dow, US). Silica and agent of silicone were mixed at a ratio of 10:1 and degassed using the planetary mixer (Kurabo Industries Ltd, Japan) for ten minutes until it formed a uniform mixture.

Top-Layer moulding: A 3D printed 75 × 25 × 2 mm mould containing six of 7 × 7 × 2 mm raised cubes was used to fabricate the top layer which has six bottomless primary wells. The mould was made out of Acrylonitrile Butadiene Styrene (ABS). The design was set up and printed using SolidWorks (U.S.A.) and Ultimaker 2 (Ultimaker B.V., Utrecht). The mould was prepared with gas silanization using 100 µl of Trichloro (1 H,1 H,2 H,2 H-perfluorooctyl) silane solution (Sigma-Aldrich, Germany) for 30 min in a salinization desiccator. PDMS was poured into the mould on a levelled table and cured on a hot plate at 80 °C for 30 min. The bottom thin layer was prepared by laser engraving a spin-coated thin layer of PDMS. A 200 µm thin layer of PDMS was spin-coated on a polymethyl methacrylate sheet by adding ~ 8 ml of PDMS on to the middle of the wafer and spinning at 1500 rpm for 60 s at RT in the wafer spin coater (APT Polos, Netherland). The PDMS thin layer was cured on the hot plate at 80 °C for ten minutes.

Bottom-layer engraving: Dimensions for six sets of 20 circular secondary wells of diameter 0.15–0.20 mm and 2 mm depth were set up using Ruby® laser software (Trotec, Australia) and engraved into the PDMS thin layer using a Speedy 360 laser engraver (Trotec, Australia). Engraved wells were examined for structural integrity and regularity using an optical microscope (Zeiss, Germany) at 4× magnification.

Assembly, cleaning and sterilization: Before attaching the microwell assembly on a 75 × 25 × 0.5 mm microscopic quartz slide (Emgrid Pty Ltd, Australia), both top and bottom PDMS layers and the quartz slide were cleaned using 70% ethanol. Bonding surfaces of both top and bottom PDMS layers were activated using oxygen plasma cleaner (PIC Scientific, U.S.A.), aligned and bonded together to assemble the microwell. Similarly, bonding surfaces of the microwell and the quartz slide were activated using the oxygen plasma cleaner, aligned and bonded together to assemble the complete microwell device. The final product was cured in the dry oven at 80 °C for 20 min. Microwells were rinsed with 70% ethanol and subsequently washed with sterile PBS before use. The produced microwell devices can also be sterilized by autoclaving at 121 °C for 25 min.

Collection of eggs from gravid female mites into the microwells

Scabietic skin crusts were collected from a porcine scabies model[24] maintained at the Queensland Animal Science Precinct, University of Queensland, Brisbane, Australia and transported to the QIMR Berghofer, Herston, Australia within two hours of sampling. Skin crusts were placed on glass Petri dishes and exposed to a light source for 20 minutes to facilitate mites crawling out of the crusts. Batches of 200 *S. scabiei* gravid female mites were individually hand-picked under a stereo binocular dissecting microscope (Nikon, Japan) at 3.5× zoom magnification and placed on glass Petri dishes with 50 µl of olive oil (REMANO® extra virgin olive oil, Remano, Italy) at RT. An average of ten freshly laid eggs were collected within 30 minutes per dish. Secondary wells were filled with olive oil using a one millilitre syringe with a 26G×1/2" needle. Among several mediums trialled in our laboratory, olive oil presented optimum survival of *S. scabiei* eggs[13]. Freshly laid eggs were individually picked from the egg pool using an insect pin (Roboz Surgical Instrument Co., USA) and placed at the bottom of each micro well under a stereo binocular dissecting microscope (Nikon, Japan) at 3.5× zoom magnification.

Time-lapse microscopy of *S. scabiei* eggs

Time-lapse microscopy was performed in two independent experiments. Two independent batches of 20 freshly laid eggs each (n = 40) were analysed. Twenty individual eggs were loaded into a microwell device at a time. Phase contrast images were captured using a 20× objective lens (N.A. 0.40) on the EVOS™ FL Auto 2 inverted microscope (Invitrogen, Thermo Fischer Scientific Corporation, USA) equipped with a motorized X-Y-Z stage. The microscope was housed in a commercial incubator (HeraCell VIOS 160i, Thermo Fisher) with capability to actively maintain embryos at 37 °C temperature, 5% CO_2, 20% O_2 with 85–90% humidity. The microwell device was mounted on the automated stage and the X-Y position of each egg within the microwell was marked in the EVOS acquisition software. A time-lapse imaging sequence was programmed to acquire a z-stack of each egg consisting of 7 optical planes (total range of 55 µm) every 15 min for a total of 72 h. Raw image data was saved as individual image files for each egg, z-slice and time-point in 16-bit TIFF format. One imaging experiment typically yielded a dataset of approximately 40,460 images. This high-volume dataset was reconstructed and processed into compact, analysis-ready files using the open-source bio-image processing and analysis software Fiji[27]. A macro script was developed by the Microscopy facility at QIMR Berghofer to batch process the compilation of the raw image data into full time-lapse movies of each egg for visualisation and tracking of egg development (macro script available upon request).

Data acquisition and statistical analysis

Time-lapse images of 40 eggs were analyzed to identify the embryonic stages and morphological events in the *S. scabiei* eggs. Median observation times with IQR (interquartile range) of identified embryonic stages and morphological events were recorded. An interval-censored parametric survival model (accelerated failure time, lognormal distribution) was used to estimate median times to the onset of each morphological event, along with corresponding 95% confidence intervals (CIs). All analyses and visualizations were performed using R software (version 4.1.0) and the icenReg package[59].

Data availability

Time lapse movie files are available at https://doi.org/10.48610/fe96dbe.

Received: 10 April 2025; Accepted: 20 November 2025
Published online: 05 December 2025

References

1. Fernando, D. D. et al. Scabies. *Nat. Rev. Dis. Primers*. **10** (1), 74 (2024).
2. Steer, A. C. et al. High burden of impetigo and scabies in a tropical country. *PLoS Negl. Trop. Dis.* **3** (6), e467 (2009).
3. Lynar, S., Currie, B. J. & Baird, R. Scabies and mortality. *Lancet. Infect. Dis*. **17** (12), 1234 (2017).
4. Chosidow, O. & Hay, R. J. Control of scabies and secondary impetigo: optimising treatment effectiveness in endemic settings. *Lancet. Infect. Dis*. **19** (5), 454–456 (2019).
5. Bernigaud, C. et al. The challenge of developing a Single-Dose treatment for scabies. *Trends Parasitol.* **35** (11), 931–943 (2019).
6. Arlian, L. G. & Morgan, M. S. A review of sarcoptes scabiei: past, present and future. *Parasites Vectors*. **10** (1), 297–297 (2017).
7. Siddig, E. E. & Hay, R. Laboratory-based diagnosis of scabies: a review of the current status. *Trans. R Soc. Trop. Med. Hyg.* **116** (1), 4–9 (2022).
8. Liu, X., Walton, S. & Mounsey, K. Vaccine against scabies: necessity and possibility. *Parasitology* **141** (6), 725–732 (2014).
9. Roberts, L. J. et al. Crusted scabies: clinical and immunological findings in seventy-eight patients and a review of the literature. *J. Infect.* **50** (5), 375–381 (2005).

10. Bernigaud, C. et al. *How To Eliminate Scabies Parasites from fomites – a High Throughput Ex Vivo Experimental Study* (Journal of the American Academy of Dermatology, 2019).
11. Wolstenholme, A. J. & Rogers, A. T. Glutamate-gated chloride channels and the mode of action of the avermectin/milbemycin anthelmintics. *Parasitology* **131** (S1), S85–S95 (2005).
12. Wolstenholme, A. J. Glutamate-gated chloride channels. *J. Biol. Chem.* **287** (48), 40232–40238 (2012).
13. Bernigaud, C. et al. In vitro ovicidal activity of current and under-development scabicides: which treatments kill scabies eggs? *Br. J. Dermatol.* **182** (2), 511–513 (2020).
14. Bernigaud, C. et al. Preclinical study of Single-Dose Moxidectin, a new oral treatment for scabies: Efficacy, Safety, and pharmacokinetics compared to Two-Dose Ivermectin in a Porcine model. *PLoS Negl. Trop. Dis.* **10** (10), e0005030 (2016).
15. Aussy, A. et al. Risk factors for treatment failure in scabies: a cohort study. *Br. J. Dermatol.* **180** (4), 888–893 (2019).
16. Williams, C. & Fuller, L. C. Why does scabies treatment fail? *Br. J. Dermatol.* **180** (4), 710–711 (2019).
17. Shelley, W. B. & Shelley, E. D. Scanning electron microscopy of the scabies burrow and its contents, with special reference to the sarcoptes scabiei egg. *J. Am. Acad. Dermatol.* **9** (5), 673–679 (1983).
18. Lange, A. B. & Sokolova, T. V. Development of the larvae inside the body of the itch mites sarcoptes scabiei (L.) (Sarcoptidae) and the ontogenetic level of eclosion in mites of the order Acariformes. Nauchnye Doklady Vysshei Shkoly. *Biol. Nauki*, **1992**(5), 63–71 (1992).
19. Mazzini, M. & Baiocchi, R. Fine morphology of the egg-shell of sarcoptes scabiei (L.) (Acarina: Sarcoptidae). *Int. J. Parasitol.* **13** (5), 469–473 (1983).
20. Kim, K. T., Lee, S. H. & Kwak, D. Sarcoptic mange in captive maras: the first known outbreak and complete recovery with colony-wide acaricide treatment. *J. Vet. Med. Sci.* **77** (5), 593–595 (2015).
21. Rahdar, M., Vazirianzadeh, B. & Maraghi, S. *A case report of sarcoptes scabiei infection in Ahwaz, Iran*. *Iran. J. Arthropod-Borne Dis.*, 2. (2008).
22. Head, E. S. et al. Sarcoptes scabiei in histopathologic sections of skin in human scabies. *Arch. Dermatol.* **126** (11), 1475–1477 (1990).
23. Fernando, D. D. et al. An RNA interference tool to silence genes in sarcoptes scabiei eggs. *Int. J. Mol. Sci.* **23** (2), 873 (2022).
24. Mounsey, K. et al. A tractable experimental model for study of human and animal scabies. *PLoS Negl. Trop. Dis.* **4** (7), e756 (2010).
25. Fain, A. Epidemiological problems of scabies. *Int. J. Dermatol.* **17** (1), 20–30 (1978).
26. Arlian, L. G. Biology, host Relations, and epidemiology of sarcoptes scabiei. *Ann. Rev. Entomol.* **34** (1), 139–159 (1989).
27. Schindelin, J. et al. Fiji: an open-source platform for biological-image analysis. *Nat. Methods*. **9** (7), 676–682 (2012).
28. Venkitachalam, S. et al. Density-dependent selection in drosophila: evolution of egg size and hatching time. *J. Genet.* **101** (1), 13 (2022).
29. Rivera-Pomar, R. & Jäckle, H. From gradients to stripes in drosophila embryogenesis: filling in the gaps. *Trends Genet.* **12** (11), 478–483 (1996).
30. Mittmann, B. & Wolff, C. Embryonic development and staging of the cobweb spider parasteatoda tepidariorum C. L. Koch, 1841 (syn.: Achaearanea tepidariorum; Araneomorphae; Theridiidae). *Dev. Genes Evol.* **222** (4), 189–216 (2012).
31. McGregor, A. P. et al. Cupiennius salei and Achaearanea tepidariorum: spider models for investigating evolution and development. *Bioessays* **30** (5), 487–498 (2008).
32. Hinne, I. A. et al. Early embryonic development in the tick Ixodes scapularis suggests syncytial organization and cellularization before blastoderm formation. *Evodevo* **16** (1), 4 (2025).
33. Santos, V. T. et al. The embryogenesis of the tick rhipicephalus (Boophilus) microplus: the establishment of a new chelicerate model system. *Genesis* **51** (12), 803–818 (2013).
34. Dearden, P. K., Donly, C. & Grbic, M. Expression of pair-rule gene homologues in a chelicerate: early patterning of the two-spotted spider mite Tetranychus urticae. *Development* **129** (23), 5461–5472 (2002).
35. Wolff, C. & Hilbrant, M. The embryonic development of the central American wandering spider Cupiennius salei. *Front. Zool.* **8** (1), 15–15 (2011).
36. Scholtz, G. & Wolff, C. Arthropod embryology: cleavage and germ band development, in Arthropod Biology and Evolution, A. Minelli, G. Boxshall, and G. Fusco, Editors. Springer: Berlin, Heidelberg. 63–89. (2013).
37. Laumann, M. et al. First cleavages, preblastula and blastula in the parthenogenetic mite archegozetes longisetosus (Acari, Oribatida) indicate holoblastic rather than superficial cleavage. *Arthropod Struct. Dev.* **39** (4), 276–286 (2010).
38. Laumann, M., Norton, R. A. & Heethoff, M. *Acarine embryology: Inconsistencies, artificial results and misinterpretations*. Vol. 82. 217–235. (2010).
39. Chetverikov, P. E. & Desnitskiy, A. G. A study of embryonic development in eriophyoid mites (Acariformes, Eriophyoidea) with the use of the fluorochrome DAPI and confocal microscopy. *Exp. Appl. Acarol.* **68** (1), 97–111 (2016).
40. Chaw, R. C., Vance, E. & Black, S. D. Gastrulation in the spider Zygiella x-notata involves three distinct phases of cell internalization. *Dev. Dyn.* **236** (12), 3484–3495 (2007).
41. Akiyama-Oda, Y. & Oda, H. Early patterning of the spider embryo: a cluster of mesenchymal cells at the cumulus produces Dpp signals received by germ disc epithelial cells. *Development* **130** (9), 1735–1747 (2003).
42. Sinico, T. E. et al. Notes on the embryological development of the brevipalpus yothersi (Acari: Tenuipalpidae). *Acarologia* **62** (1), 113–119 (2022).
43. Yastrebtsov, A. Embryonic development of gamasid mites (Parasitiformes: Gamasida). *Int. J. Acarol.* **18** (2), 121–141 (1992).
44. Janssen, R., Pechmann, M. & Turetzek, N. A chelicerate Wnt gene expression atlas: novel insights into the complexity of arthropod Wnt-patterning. *EvoDevo* **12** (1), 12 (2021).
45. Schmitt-Engel, C. et al. The iBeetle large-scale RNAi screen reveals gene functions for insect development and physiology. *Nat. Commun.* **6**, 7822 (2015).
46. Pechmann, M. Embryonic development and secondary axis induction in the Brazilian white knee tarantula acanthoscurria geniculata, C. L. Koch, 1841 (Araneae; Mygalomorphae; Theraphosidae). *Dev. Genes Evol.* **230** (2), 75–94 (2020).
47. Chong, J., Amourda, C. & Saunders, T. E. Temporal development of drosophila embryos is highly robust across a wide temperature range. *J. Royal Soc. Interface*. **15** (144), 20180304 (2018).
48. Machner, J. & Scholtz, G. A scanning electron microscopy study of the embryonic development of pycnogonum litorale (Arthropoda, Pycnogonida). *J. Morphol.* **271** (11), 1306–1318 (2010).
49. Abidalla, M. & Battaglia, D. *Novel Staining Procedures for Whole Mount Preparations of Greater Wax Moth (Galleria mellonella) Embryos: Toluidine blue-rhodamine B, Plus Calcofluor White* Vol. 94, p. 108–114 (Biotechnic & Histochemistry, 2019). 2.
50. Müller, H. A. Immunolabeling of embryos. *Methods Mol. Biology*. **420**, 207–218 (2008).
51. Kobayashi, Y., Suzuki, H. & Ohba, N. *Formation of a spherical germ rudiment in the egg of a glow-worm, Rhagophthalmus ohbai Wittmer (Coleoptera, Rhagophthalmidae), and its phylogenetic implications*. Proceedings of Arthropodan Embryological Society of Japan, 36: pp. 1–5. (2001).
52. Kuntz, S. G. & Eisen, M. B. Drosophila embryogenesis scales uniformly across temperature in developmentally diverse species. *PLoS Genet.* **10** (4), e1004293 (2014).
53. Janssen, R. et al. Embryonic expression patterns and phylogenetic analysis of Panarthropod Sox genes: insight into nervous system development, segmentation and gonadogenesis. *BMC Evol. Biol.* **18** (1), 88 (2018).
54. Ubara, M. & Osakabe, M. Suspension of egg hatching caused by high humidity and submergence in spider mites. *Environ. Entomol.* **44** (4), 1210–1219 (2015).

55. Fukuse, K. & Yano, S. Delayed mite hatching in response to mechanical stimuli simulating egg predation attempts. *Sci. Rep.* **9** (1), 13395 (2019).
56. Arlian, L. G. & Vyszenski-Moher, D. L. Life cycle of sarcoptes scabiei var. Canis. *J. Parasitol.* **74** (3), 427–430 (1988).
57. Ljunggren, E. L. *Molecular Analysis of Sarcoptes Scabiei* (Department of Biomedical Sciences and Veterinary Public Health, 2005).
58. Muluneh, M. & Issadore, D. Hybrid soft-lithography/laser machined microchips for the parallel generation of droplets. *Lab. Chip.* **13** (24), 4750–4754 (2013).
59. Team, R. C. *R: A language and environment for statistical computing.* ; (2021). Available from: https://www.R-project.org/

Acknowledgements
The authors thank Dr Bingzhao Xia and Dr Juan Li at the Australian National Fabrication Facility - Queensland Node (ANFF-Q), Australian Institute for Bioengineering and Nanotechnology, University of Queensland, St. Lucia for the training and help with optimization, establishment and fabrication of the microgrid; Mr Hieng Lu for help with fabrication of the microgrid; Dr Nigel Waterhouse of the Scientific Services, QIMR Berghofer for his help with optimizing the time-lapse microscopy method and Ms Chelsea Baker, Ms Sheree Boisen, Mr Scott Cullen and Dr Milou Dekkers at the Queensland Animal Science Precinct, University of Queensland, Gatton Campus, Australia, for maintaining the porcine *S. scabiei* model.

Author contributions
G.R.S., D.D.F. and K.F. conceived the experiment(s), G.R.S. conducted the experiment(s) with advice from D.D.F., M.K.J., T.H.N. and K.F. G.R.S., S.O., G.H., D.D.F. and K.F. analysed the results. G.R.S. and K.F. wrote the manuscript. All authors reviewed the manuscript.

Funding
Support from the National Health and Medical Research Council (NHMRC) of Australia (KF, DF) is gratefully acknowledged. KF held an NHMRC Senior Research Fellowship (1154805), and the project was funded by NHMRC grant 1163354. G.S. was supported by a PhD scholarship from University of Queensland, Australia and a PhD top up award from QIMR Berghofer, Australia. The funders had no role in study design, data collection and/or analysis, decision to publish, or the preparation of the manuscript.

Declarations

Ethics approval and content od participate
Skin crusts samples required for the experiments were obtained from the porcine scabies model maintained at the Queensland Animal Science Precinct (QASP) – University of Queensland (UQ), Gatton. The study was approved by the UQ and QIMRB Animal Ethics Committees, 2021/AE001015 and QIMR P630. Animal handling, care and the procedures involved in this study were followed according to the Animal Care and Protection Act and in compliance with the Australian code of practice for the care and use of animals for scientific purposes, outlined by the Australian National Health and Medical Research Council (NHMRC).

Competing interests
The authors declare no competing interests.

Additional information
Supplementary Information The online version contains supplementary material available at https://doi.org/10.1038/s41598-025-29910-6.

Correspondence and requests for materials should be addressed to K.F.